Stretchable Photonic 'Fermi Arcs' in Twisted Magnetized Plasma

Lingbo Xia[1, 2*], Wenlong Gao[1*], Biao Yang[1], Qinghua Guo[1,3], Hongchao Liu[1], Jiaguang Han[2], Weili Zhang[2], Shuang Zhang[1, 2†]

[1]*School of Physics & Astronomy, University of Birmingham, Birmingham, B15 2TT, UK*

[2]*Center for Terahertz Waves and College of Precision Instrument and Optoelectronics Engineering, Tianjin University, Tianjin 300072, China*

[3]*SZU-NUS Collaborative Innovation Centre for Optoelectronic Science & Technology, Key Laboratory of Optoelectronic Devices and Systems of Ministry of Education and Guangdong Province, College of Optoelectronic Engineering, Shenzhen University, Shenzhen 518060, China*

**These authors contributed equally to this work*

†*Corresponding E-mail: s.zhang@bham.ac.uk*

Abstract: Weyl points, three-dimensional linear bulk bands crossings possessing intrinsic helicities, are counterparts of magnetic monopoles in the momentum space. One of the most important features of Weyl semimetals is the presence of topologically protected non-trivial surface states at the boundary that connect between Weyl points of opposite charges. In condensed matter physics, these surface states are called Fermi arcs whose length measures the topological strength of the system. Here we theoretically show that photonic 'Fermi arcs' can exist at the interface between two magnetized plasma under static bias magnetic fields of different orientations, i.e. a twisted configuration, whereas the length of the 'Fermi arcs' can be arbitrarily stretched by varying the relative orientation and intensities of two static bias magnetic fields. Interestingly, the 'Fermi arcs' join two Weyl points of the same sign but residing on different side of the interface. Our work gives insight to the connectivity of 'Fermi arcs' between two topological semimetals and could open gateway towards tunable photonic topological systems.

Keywords: photonic 'Fermi Arcs'; strechable; Weyl point; magnetized plasma;

1. Introduction

Weyl semimetals exhibiting linear bulk bands crossings, or Weyl points, have attracted growing attentions recently [1-3]. Weyl points serve as quantized monopole charges with opposite helicities acting as sources and sinks of Berry curvature in the momentum space. The dispersion relation around the Weyl points are described by the Weyl Hamiltonian $H(\mathbf{k}) = v_x k_x \sigma_x + v_y k_y \sigma_y + v_z k_z \sigma_z$ [4], where v_i, k_i, σ_i are group velocity, momenta and Pauli matrix, respectively. Compared with the two-dimensional Dirac points described by $H(\mathbf{k}) = v_x k_x \sigma_x + v_y k_y \sigma_y$ [5], the Weyl points are highly robust since all three Pauli matrixes are included for two bands description in the Weyl Hamiltonian. In other words, Dirac points can be easily gapped by a mass term proportional to σ_z, whereas Weyl points can only be annihilated by the merging of two Weyl points of opposite signs [4]. In general, the existence of Fermi arcs is an important hall mark of the nontrivial bulk properties [6-10]. The opposite helical Weyl points are connected by an exotic open Fermi arc at the interface and the length of the Fermi arc measures the topological strength [11].

By breaking either inversion symmetry or time reversal symmetry, Weyl points have been reported to exist not only in condensed matter systems [12-16], but also in classical photonic and phononic systems [17-27]. Two kinds of Weyl points, type-I and type-II, were distinguished by the density of states and Fermi surface [15]. Recently, it has been shown that a photonic plasmon Weyl point, which is right at the transition between type-I and type-II, could take place in magnetized plasma [23,28]. The degeneracy is protected by the orthogonality between the longitudinal plasma mode and helical propagating mode. At the interface between the magnetized plasma and a normal

medium such as vacuum or perfect electrical conductor, there exists the 'Fermi arcs' that connects two Weyl points of opposite helicities. Thus far, nontrivial surface states, or" 'Fermi arcs', have been investigated exclusively at the interface between a topological semimetal and a topologically trivial insulator. However, 'Fermi arcs' between two distinct topological semimetals have not been studied. Here, we report the photonic 'Fermi arcs' at the boundary of two photonic magnetized plasma 'Weyl semimetals'. By tuning the relative magnetization direction and intensities of the two interfacial plasma, the 'Fermi arcs' could be stretched arbitrarily. Furthermore, a non-conventional 'Fermi arc' connectivity feature, i.e., 'Fermi arcs' joining two Weyl points of the same sign but residing on different side of the interface, is observed, which brings a new insight to the connectivity of the 'Fermi arcs'.

2. RESULTS AND DISCUSSION

The configuration of the twisted magnetized plasma is shown in Fig. 1a, where the two magnetized plasma materials are denoted by M_A and M_B. For M_A with static bias magnetic field $\mathbf{B_1}$ along z axis, the permittivity can be written as a 3-by-3 matrix $\boldsymbol{\varepsilon}_{MA} = [\varepsilon_1, i\varepsilon_2, 0; -i\varepsilon_2, \varepsilon_1, 0; 0, 0, \varepsilon_3]$, where $\varepsilon_1 = \varepsilon_\infty - \omega_p^2(\omega^2 + i\gamma\omega)/[(\omega^2 + i\gamma\omega)^2 - \omega^2\omega_{ca}^2]$, $\varepsilon_2 = \omega\omega_{ca}\omega_p^2/[(\omega^2 + i\gamma\omega)^2 - \omega^2\omega_{ca}^2]$, $\varepsilon_3 = \varepsilon_\infty - \omega_p^2/(\omega^2 + i\gamma\omega)^2$, and ω, ω_{ca}, ω_p and γ are the angular frequency, cyclotron resonance frequency, electron plasma frequency and damping frequency, respectively. The static bias magnetic field $\mathbf{B_2}$ of M_B is in the x-z plane making an angle $-\theta$ with the z axis. The permittivity $\boldsymbol{\varepsilon}_{MB}$ of M_B can be obtained through a coordinate transformation from $\boldsymbol{\varepsilon}_{MA}$. For simplicity, we first consider the case when $\mathbf{B_1}$ and $\mathbf{B_2}$ have the same magnitude by setting $\omega_{ca} = \omega_{cb} = 1.2\omega_p$. The loss can be neglected when dealing with cold plasma with a low enough electron density. With this simplification, a

9-by-9 Hamiltonian matrix can be constructed to describe the band structure of magnetized plasma, with the vector space consisting of the electric field, the magnetic field and the electrons' velocity field [23]. The band structure of the bulk states of M_A is shown in Fig. 1b. The band structure of M_B is identical to M_A but rotated by an angle θ in the x-z plane relative to that of M_A. At the plasma frequency $\omega = \omega_p$, there exist a pair of Weyl points along the k_z axis in momentum space located at $K_z^{Weyl} = \pm\sqrt{\omega_c/(\omega_c - \omega_p)}$. Here, the momentum vectors are given in unit of $k_p = \omega_p/c$, where c is the speed of light in vacuum. Here, we denote the positive and negative Weyl points in $M_{A(B)}$ by $W_{A(B)+}$ and $W_{A(B)-}$, respectively. The surface states are calculated by applying the boundary condition of transverse components of electric and magnetic fields (see Supplementary Material) [29-31]. As is well known, 'Fermi arcs' at the boundaries of 'Weyl semimetals' connect the projections of Weyl points with opposite helicities. However, in our configuration, the fact that Weyl materials reside on both side of the interface may render a different 'Fermi arcs' connectivity between Weyl points of different materials across the interface, with the same helicity. Fig. 1c to 1e show the bulk states of M_A (denoted by black curves) and M_B (denoted by blue curves) and surface states (denoted by red curves) at the boundary between M_A and M_B with $\theta = \pi/4$ at the frequencies of $\omega = 0.99\omega_p$, $\omega = \omega_p$ and $\omega = 1.01\omega_p$ respectively. At the Weyl degeneracy frequency (Fig. 1d), one 'Fermi arc' directly connects between W_{A-} and W_{B-}, while the other 'Fermi arc' connects W_{A+} and W_{B+} with part merged into the bulk states in the middle. Slightly below (Fig. 1c) and above (Fig. 1e) the Weyl frequency, the 'Fermi arcs' show very similar configuration as that in Weyl frequency despite a dramatic change in the bulk equifrequency surface.

'Fermi arcs' Connectivity Features: In order to understand the connectivity of the surface states in the momentum space, we add an air slab between M_A and M_B as shown in Fig. 2a. The surface states at the air-M_A and air-M_B interfaces can couple with each other via the finite-thickness air slab. When the thickness of the air slab is $h = 4\lambda$ (λ is the wavelength at Weyl degeneracy frequency in vacuum), coupling between the surface states at air-M_A and air-M_B interface is too weak to be negligible. Consequently, the two 'Fermi arcs', one connecting from W_{A+} to W_{A-} and the other connecting from W_{B+} to W_{B-}, just intersect with each other as a simple superposition of the surface states at two air-magnetized plasma interface [31], as shown in Fig. 2b. When the thickness of the air slab decreases to $h = 2\lambda$, the coupling between the surface states becomes stronger, and a finite gap in momentum space is opened up where the two 'Fermi arcs' meet. Notably, the gap-opening has rerouted the 'Fermi arcs' to connect the Weyl points of different magnetized plasma across the interface with the same helicity that is W_{A+} to W_{B+} and W_{A-} to W_{B-}, as shown in Fig. 2c. By further reducing the thickness of the air slab to $h = 0.2\lambda$, the 'Fermi arc' connecting between the two negative Weyl points becomes less curved, while the 'Fermi arc' between the two positive Weyl points starts to merge into the circular bulk state, as shown in Fig. 2d. It should be noted that this already closely resembles the 'Fermi arcs' connectivity when the thickness is zero as shown in Fig. 1d.

This 'Fermi arcs' connection between two Weyl points of different materials across the interface but with the same helicity can also be understood by the effective Hamiltonian around the Weyl point for the evanescent eigen-states decaying away from the interface, which reads (see Supplementary Material):

$$\begin{bmatrix} Mk_z & N(k_x + \sigma v|k_x|) \\ N(k_x - \sigma v|k_x|) & 0 \end{bmatrix}, \quad (1)$$

where $\sigma = \pm 1$ represents the helicity of the Weyl point, $\upsilon = \mathrm{sgn}(-ik_y)$ indicates the decaying direction of the surface state and consequently on which side of the interface the Weyl point is located. M and N are positive constants determined by ω_p and ω [23]. The eigen-state of the above effective Hamiltonian is expressed as $|\sigma, \nu\rangle = [k_x + \sigma\nu|k_x|, -k_z M/N]$. It is apparent that $|+1,+1\rangle$ and $|-1,-1\rangle$ (as well as $|-1,+1\rangle$ and $|+1,-1\rangle$) share the same eigen-state. Here, the decaying state for W_{A+} is described by $|+1,+1\rangle$, and $|-1,-1\rangle$ represents a decaying state of the "mirror image" of W_{A+}. This "mirror image", denoted as W_{B-}^{A+}, can be viewed as a pseudo Weyl point with opposite helicity corresponding to W_{A+} on the other side of the interface. Therefore, 'Fermi arcs' join two Weyl points of same helicity residing on different side of the interface (e.g. $W_{A+} \leftrightarrow W_{B+}$) in our case, can be understood as the well-known positive-to-negative connectivity (e.g. $W_{B-}^{A+} \leftrightarrow W_{B+}$). Similar analysis can be applied to the connectivity between W_{A-} and W_{B-}. The other possibility to link W_{A+} (W_{A-}) to W_{B-} (W_{B+}) is forbidden since effectively they possess the same helicity after the mirror operation.

Stretchable 'Fermi arcs'. The twisted magnetized plasma configuration not only introduces the exotic 'Fermi arcs' connectivity between two Weyl points of the same helicity, but also enables versatile stretchable 'Fermi arcs' by simply tuning the orientation or the magnitude of the two applied static magnetic field, which is not readily realizable in usual configuration of 'Weyl semimetal' interfacing with trivial insulators. Firstly, we keep the magnitude of the magnetic fields the same as $\omega_{ca} = \omega_{cb} = 1.2\omega_p$ and vary their relative orientation angle θ from 0 to 2π with a step of $\pi/4$, as shown in Fig. 3a to 3h. In Fig. 3a, the system becomes a homogeneous bulk magnetized plasma for $\theta = 0$, thus no 'Fermi arcs' exists. For $\theta \neq 0$, an interface is

formed between M_A and M_B, resulting in 'Fermi arcs' connecting between the corresponding Weyl points [1]. As shown in Fig. 3b to 3d, for θ varying from $\pi/4$ to $3\pi/4$, one 'Fermi arc' always makes a direct connection between the two weyl points of negative topological charge, while the other 'Fermi arc' connects between two positive Weyl points indirectly through the circular bulk states. Particularly, in the case of $\theta = \pi$ (Fig. 3e), Weyl points of the two magnetized plasma with opposite helicity coincide in the momentum space. It is found that any contours in the momentum space encircling W_{A+} (W_{A-}) and W_{B-} (W_{B+}) gains Chern number of ± 2 [1]. Thus there must exist two 'Fermi arcs' terminating into the degeneracy point. Fig. 3e shows that one 'Fermi arc' approaches the bulk plasma mode and runs vertically into the circular bulk state, whereas the other 'Fermi arc' which is a transverse electric mode makes a curved trajectory around the circular bulk mode and connects between the two degeneracy points. This can be easily understood by a symmetry analysis. The M_A and M_B are mirror symmetrical across the boundary in the case of $\theta = \pi$. Given an in-plane eigenstate $[E_{\parallel}, H_{\parallel}]$ of M_A, the $[E_{\parallel}, -H_{\parallel}]$ is also an eigenstate of M_B due to the mirror symmetry. Therefore, when matching the boundary condition, either $E_{\parallel} = 0$ or $H_{\parallel} = 0$ respects to the transverse electric mode and longitudinal mode separately. When the angle θ changes from $5\pi/4$ to $7\pi/4$, the two positive topological charges are connected directly by a 'Fermi arc', while the two negative charges are connected indirectly by a 'Fermi arc' running through the circular bulk state, as show in Fig. 3f to 3h.

Next, we fix the relative orientation angle θ and the magnitude of static magnetic field in M_A with $\omega_{ca} = 1.2\omega_p$, and change the magnitude of the applied static magnetic field of M_B, i.e., change ω_{cb} from $1.2\omega_p$ to ω_p. As shown in Fig. 3i to

3l, the lengths of the 'Fermi arcs' are gradually stretched when ω_{cb} is reduced. When ω_{cb} approaches ω_p, the locations of W_{B+} and W_{B-} move towards infinitely large $\mathbf{k}$. Remarkably, the length of the 'Fermi arcs' goes to infinite, resulting in arbitrarily large topological strength.

Selectively Excited 'Fermi Arcs'. Finally we show that the 'Fermi arcs' can be selectively excited by a circular dipole emitter placed at the interface. Here, we present the simulated electrical field intensity distribution at the interface between M_A and M_B with an electrical dipole located at the center. The simulated configuration is the same as Fig. 1a, and the bulk states and 'Fermi arcs' in the case of $\theta = \pi/4$ are shown in Fig. 4a. The black arrows denoted by $\mathbf{S_1}$, $\mathbf{S_2}$ and $\mathbf{S_3}$ in Fig. 4a indicate the main direction of Poynting vectors of the three separate 'Fermi arcs', respectively. We added a small loss to M_A and M_B with $\gamma = 0.01\omega_p$ to give a finite band width of the surface waves to allow better excitation of them when simulated in COMSOL MULTIPHYSICS. Fig. 4b to 4d show the simulated electrical intensity $|\mathbf{E}|$ distribution excited by circularly polarized dipole given by $\mathbf{p_1} = [i\cos\pi/8, 1, i\sin\pi/8]$, $\mathbf{p_2} = [i\cos 7\pi/8, 1, i\sin 7\pi/8]$ and $\mathbf{p_3} = [i\cos 11\pi/8, 1, i\sin 11\pi/8]$, respectively. As all the three dipole configurations lie in a vertical plane perpendicular to the interface (*x*-*z* plane), we can define an in-plane spin for each of them, given by $\boldsymbol{S} = 2Re\boldsymbol{E} \times Im\boldsymbol{E}/|\boldsymbol{E}|^2$. The spin orientations of dipole are indicated by white arrows in Fig. 4b to 4d, respectively. The surface waves can be excited along three main directions, corresponding to the normal direction of the arcs as indicated by the black arrows in Fig. 4(a). For each dipole orientation given above, unidirectional excitation of the surface state along one direction can be achieved. These selectively excited 'Fermi arcs' originate from the intrinsic spin nature of the surface states [32].

3. Conclusions

In conclusion, we studied the ‘Fermi arcs’ connecting projections of Weyl points between two topological nontrivial magnetized plasma with different orientations of the applied magnetic field. The system represents an interface formed by two distinct topological ‘Weyl semimetals’, which has been rarely investigated in literatures. We discovered unconventional ‘Fermi arcs’ connectivity between two topological ‘Weyl semimetal’, namely, they connect between Weyl degeneracies of the same sign but from different sides of the interface. By controlling the relative orientation and the magnitudes of the applied magnetic fields, the ‘Fermi arcs’ can be arbitrarily stretched and compressed. This dynamically tunable photonic topological Weyl medium may greatly expand the optical functionalities of existing photonic systems.

Acknowledgements

We acknowledge the support from ERC Consolidator Grant (TOPOLOGICAL), Horizon 2020 Action (Project No. 734578), and the Chinese Scholarship Council Grant No. 201606250059, (LX).

References

[1] X. Wan, A. M. Turner, A. Vishwanath & S. Y. Savrasov, Phys. Rev. B **83**, 205101 (2011).

[2] A. A. Burkov & L. Balents, Phys. Rev. Lett. **107**, 127205 (2011).

[3] N. P. Armitage, E. J. Mele & A. Vishwanath, arXiv:1705.01111 [cond-mat.str-el] (2017).

[4] W. Hermann. Gesammelte Abhandlungen. (American Philosophical Society, 1943).

[5] H. Weng, C. Fang, Z. Fang, B. A. Bernevig & X. Dai, Phys. Rev. X **5**, 011029 (2015).

[6] A. M. Essin & V. Gurarie, Phys. Rev. B **84**, 125132 (2011).

[7] G. M. Graf & M. Porta, Commun. Math. Phys. **324**, 851-895 (2013).

[8] M. G. Silveirinha, Phys. Rev. B **92**, 125153 (2015).

[9] M. G. Silveirinha, Phys. Rev. B **94**, 205105 (2016).

[10] M. G. Silveirinha, Phys. Rev. B **95**, 115103 (2017).

[11] T.-R. Chang, S.-Y. Xu, G. Chang, C.-C. Lee, S.-M. Huang, B. Wang, G. Bian, H. Zheng, D. S. Sanchez, I. Belopolski, N. Alidoust, M. Neupane, A. Bansil, H.-T. Jeng, H. Lin & M. Zahid Hasan, Nature Commun **7**, 10639 (2016).

[12] S.-Y. Xu, I. Belopolski, N. Alidoust, M. Neupane, G. Bian, C. Zhang, R. Sankar, G. Chang, Z. Yuan, C.-C. Lee, S.-M. Huang, H. Zheng, J. Ma, D. S. Sanchez, B. Wang, A. Bansil, F. Chou, P. P. Shibayev, H. Lin, S. Jia & M. Z. Hasan, Science **349**, 613 (2015).

[13] B. Q. Lv, N. Xu, H. M. Weng, J. Z. Ma, P. Richard, X. C. Huang, L. X. Zhao,

G. F. Chen, C. E. Matt, F. Bisti, V. N. Strocov, J. Mesot, Z. Fang, X. Dai, T. Qian, M. Shi & H. Ding, Nat. Phys. **11**, 724-727 (2015).

[14] S.-Y. Xu, N. Alidoust, I. Belopolski, Z. Yuan, G. Bian, T.-R. Chang, H. Zheng, V. N. Strocov, D. S. Sanchez, G. Chang, C. Zhang, D. Mou, Y. Wu, L. Huang, C.-C. Lee, S.-M. Huang, B. Wang, A. Bansil, H.-T. Jeng, T. Neupert, A. Kaminski, H. Lin, S. Jia & M. Zahid Hasan, Nat Phys **11**, 748-754 (2015).

[15] A. A. Soluyanov, D. Gresch, Z. Wang, Q. Wu, M. Troyer, X. Dai & B. A. Bernevig, Nature **527**, 495-498 (2015).

[16] C. Fang, L. Lu, J. Liu & L. Fu, Nat Phys **12**, 936-941 (2016).

[17] L. Lu, L. Fu, J. D. Joannopoulos & M. Soljacic, Nat Photon **7**, 294-299 (2013).

[18] M. Xiao, W.-J. Chen, W.-Y. He & C. T. Chan, Nat Phys **11**, 920-924 (2015).

[19] L. Lu, Z. Wang, D. Ye, L. Ran, L. Fu, J. D. Joannopoulos & M. Soljačić, Science **349**, 622 (2015).

[20] M. Xiao, Q. Lin & S. Fan, Phys. Rev. Lett. **117**, 057401 (2016).

[21] Z. Yang & B. Zhang, Phys. Rev. Lett. **117**, 224301 (2016).

[22] W.-J. Chen, M. Xiao & C. T. Chan, Nature Commun **7**, 13038 (2016).

[23] W. Gao, B. Yang, M. Lawrence, F. Fang, B. Béri & S. Zhang, Nature Commun **7**, 12435 (2016).

[24] Q. Lin, M. Xiao, L. Yuan & S. Fan, Nature Commun **7**, 13731 (2016).

[25] J. Noh, S. Huang, D. Leykam, Y. D. Chong, K. P. Chen & M. C. Rechtsman, Nat Phys **13**, 611-617 (2017).

[26] B. Yang, Q. Guo, B. Tremain, L. E. Barr, W. Gao, H. Liu, B. Béri, Y. Xiang, D. Fan, A. P. Hibbins & S. Zhang, Nature Commun **8**, 97 (2017).

[27] B. Yang, Q. Guo, B. Tremain, R. Liu, L. E. Barr, Q. Yan, W. Gao, H. Liu, Y.

Xiang, J. Chen, C. Fang, A. Hibbins, L. Lu & S. Zhang, arXiv:1709.06065 (2017).

[28] D. Jin, L. Lu, Z. Wang, C. Fang, J. D. Joannopoulos, M. Soljačić, L. Fu & N. X. Fang, Nature Commun **7**, 13486 (2016).

[29] M. D'yakonov, Sov. Phys. JETP **67**, 714-716 (1988).

[30] W. Gao, M. Lawrence, B. Yang, F. Liu, F. Fang, B. Béri, J. Li & S. Zhang, Phys. Rev. Lett. **114**, 037402 (2015).

[31] B. Yang, M. Lawrence, W. Gao, Q. Guo & S. Zhang, Sci. Rep. **6**, 21461 (2016).

[32] K. Y. Bliokh, D. Smirnova & F. Nori, Science **348**, 1448 (2015).

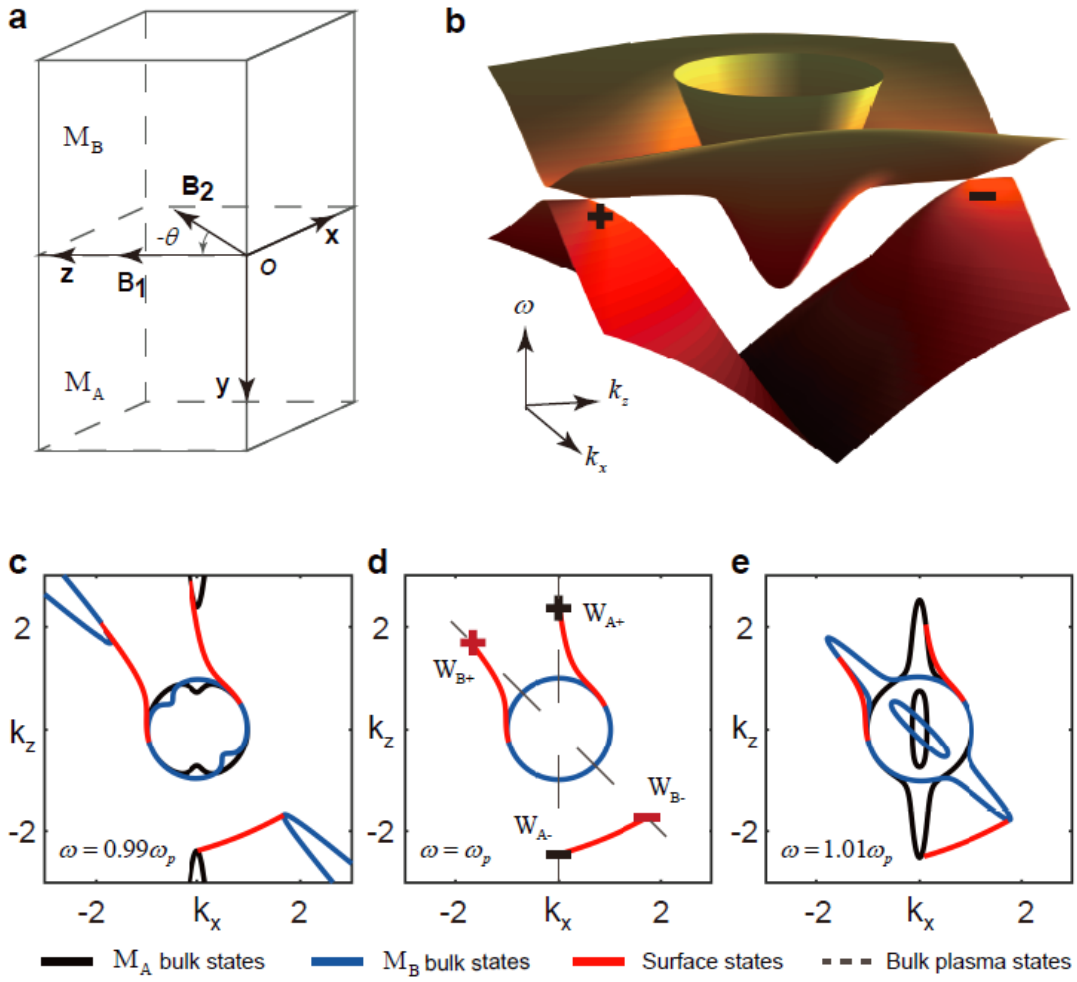

Figure 1 **(a)** Configuration of twisted magnetized plasma. M_A and M_B denote the two magnetized plasma materials, respectively. The static bias magnetic field $\mathbf{B_1}$ of M_A is along z aixs while static bias magnetic field $\mathbf{B_2}$ of M_B is in the x-z plane making an angle $-\theta$ with the z axis as indicated. The boundary between M_A and M_B lie in the x-z plane. **(b)** Band structure of M_A for $\omega_{ca} = 1.2\omega_p$ with coordinate view angle in the left bottom. The band structure of M_B is identical to M_A but rotated by an angle θ in the x-z plane relative to that of M_A. **(c)-(e)** Bulk states of M_A and M_B and surface states at the boundary between M_A and M_B at frequence of $\omega = 0.99\omega_p$, $\omega = \omega_p$ and $\omega = 1.01\omega_p$, respectively, where $\theta = \pi/4$ and $\omega_{ca} = \omega_{cb} = 1.2\omega_p$. The bulk states of M_A and M_B are represented by black and blue lines, respectively. The surface

states are shown in red lines. The dashed black lines across the Weyl point points are bulk longitudinal magnetized plasma states. W_{A+} (denoted by black '+' symbol) and W_{A-} (denoted by black '-' symbol) indicate the positive and negative Weyl point of M_A, respectively. While W_{B+} (denoted by red '+' symbol) and W_{B-} (denoted red '-' symbol) indicate the positive and negative Weyl points of M_B respectively. Part of bulk states of M_A overlapped with M_B as the blue cycle in Fig. 1d at Weyl degeneracy frequence $\omega = \omega_p$.

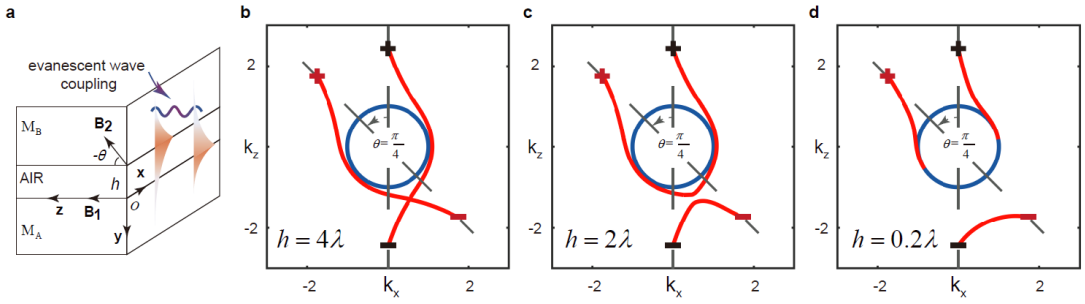

Figure 2 **(a)** An air slab with thickness of h is added between M_A and M_B and the side view shows that the coupling of the two evanescent waves existing in M_A-air boundary and M_B-air boundary. **(b)-(d)** show the change of 'Fermi arcs' in the case of $h = 4\lambda,\ 2\lambda$ and 0.2λ, respectively, where $\theta = \pi/4,\ \omega_{ca} = \omega_{cb} = 1.2\omega_p$ and $\omega = \omega_p$. The bulk states of air overlapped with bulk states M_A and M_B as the blue cycle.

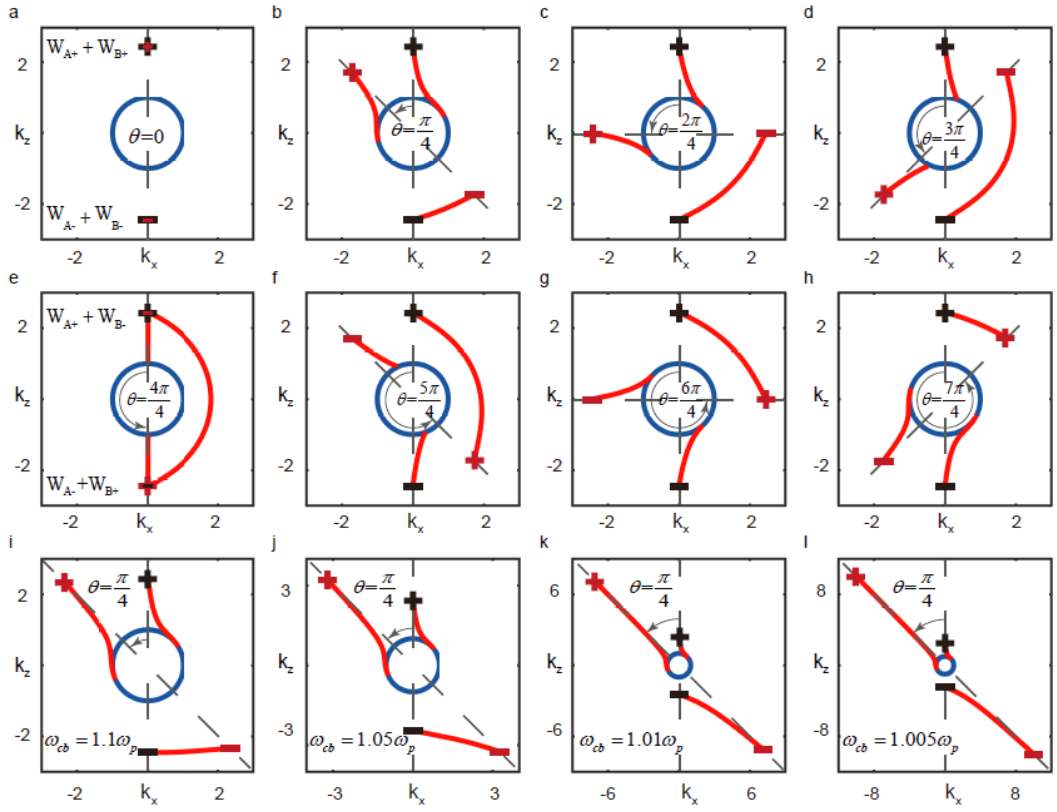

Figure 3**(a)-(h)** The 'Fermi arcs' change with relative orientation angle θ of $\mathbf{B_2}$ in the case of $\omega_{ca}=\omega_{cb}=1.2\omega_p$ at plasma frequency $\omega=\omega_p$. Two Weyl points with the same helicity degenerated in momentum space at $\theta=0$ and no 'Fermi arcs' exist. As θ vary from $\pi/4$ to $3\pi/4$, one 'Fermi arcs' directly connect from W_{A-} to W_{B-} While the 'Fermi arcs' connecting W_{A+} and W_{B+} are partly merged into the bulk states. At $\theta=\pi$, two Weyl points with the opposite helicity degenerate in momentum space and radiate two 'Fermi arcs'. As θ vary from $5\pi/4$ to $7\pi/4$, one 'Fermi arcs' connects from W_{A+} to W_{B+} directly and the other connecting W_{A-} and W_{B-} is partly merged into the bulk. **(i)-(l)** The 'Fermi arcs' vary with relative static bias magnetic intensity from $\omega_{cb}=1.1\omega_p$ to $\omega_{cb}=1.005\omega_p$ in the case of $\theta=\pi/4$ and $\omega_{ca}=1.2\omega_p$ at plasma frequency $\omega=\omega_p$. As ω_{cb} gradually approach to ω_p, the topological length of the 'Fermi arcs' can be continuously tuned from finity to infinity. Symbols black and red '+' (black and red '-') indicate two Weyl points W_{A+} and W_{B+} (W_{A-} and W_{B-})

of the same helicity degenerated in momentum space, respectively. Symbols black '+' and red '-' (red '+' and black '-') represent two Weyl points W_{A+} and W_{B-} (W_{A-} and W_{B+}) of the opposite helicity degenerated in momentum space, respectively.

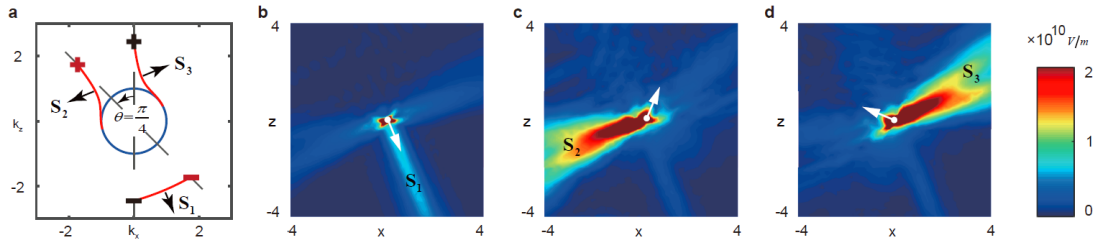

Figure 4 **(a)** Bulk states and surface states in the case of $\theta = \pi/4$ with the same condition of Fig. 3b, The black arrows denoted by $\mathbf{S_1}$, $\mathbf{S_2}$ and $\mathbf{S_3}$ indicate the direction of Poynting vector of the three separate Fermi arcs, respectively. (**b)-(d**) The simulated electrical intensity $|\mathbf{E}|$ distribution excited by circular polarized dipole with moment $\mathbf{p_1} = [i\cos\pi/8, 1, i\sin\pi/8]$, $\mathbf{p_2} = [i\cos 7\pi/8, 1, i\sin 7\pi/8]$ and $\mathbf{p_3} = [i\cos 11\pi/8, 1, i\sin 11\pi/8]$ in the case of $\theta = \pi/4$, respectively. The spin direction of the three circular dipoles is denoted by white arrows, respectively. A litter loss with $\gamma = 0.01\omega_p$ is added to give a finite band width of the surface waves for better excitation. The other parameters are set as $\omega_{ca} = \omega_{cb} = 1.2\omega_p$ and $\omega = \omega_p$.